J Arid Land (2025) 17(1): 74–92
doi: 10.1007/s40333-025-0070-2; CSTR: 32276.14.JAL.02500702

Science Press Springer-Verlag

Spatiotemporal variation and driving factors of vegetation net primary productivity in the Guanzhong Plain Urban Agglomeration, China from 2001 to 2020

LIU Yuke, HUANG Chenlu*, YANG Chun, CHEN Chen

School of Tourism & Research Institute of Human Geography, Xi'an International Studies University, Xi'an 710128, China

Abstract: Studying the spatiotemporal variation and driving mechanisms of vegetation net primary productivity (NPP) in the Guanzhong Plain Urban Agglomeration (GPUA) of China is highly important for regional green and low-carbon development. This study used the Theil-Sen trend analysis, Mann-Kendall trend test, coefficient of variation, Hurst index, and machine learning method (eXtreme Gradient Boosting and SHapley Additive exPlanations (XGBoost-SHAP)) to analyze the spatiotemporal variation of NPP in the GPUA from 2001 to 2020 and reveal its response to climate change and human activities. The results found that during 2001–2020, the averageNPP in the GPUA showed a significant upward trend, with an annual growth rate of 10.84 g C/(m²•a). The multi-year average NPP in the GPUA was 484.83 g C/(m²•a), with higher values in the southwestern Qinling Mountains and lower values in the central and northeastern cropland and built-up areas. The average coefficient of variation of NPP in the GPUA was 0.14, indicating a relatively stable state overall, but 72.72% of the study area showed weak anti-persistence, suggesting that NPP in most areas may have declined in the short term. According to XGBoost-SHAP analyses, elevation, land use type and precipitation were identified as the main driving factors of NPP. Appropriate precipitation and higher temperatures promote NPP growth, whereas extreme climates, high population density, and nighttime lighting inhibit NPP. This study has important theoretical and practical significance for achieving regional sustainable development, offers a scientific basis for formulating effective ecological protection and restoration strategies, and promotes green, coordinated, and sustainable development in the GPUA.

Keywords: net primary productivity (NPP); Theil-Sen trend analysis; machine learning; climate change; urbanization; Guanzhong Plain Urban Agglomeration (GPUA)

Citation: LIU Yuke, HUANG Chenlu, YANG Chun, CHEN Chen. 2025. Spatiotemporal variation and driving factors of vegetation net primary productivity in the Guanzhong Plain Urban Agglomeration, China from 2001 to 2020. Journal of Arid Land, 17(1): 74–92. https://doi.org/10.1007/s40333-025-0070-2; https://cstr.cn/32276.14.JAL.02500702

1 Introduction

Urbanization refers to the process of population, economic, social, and land use concentration from rural to urban areas (Lin et al., 2015). With the acceleration of global urbanization, urban expansion often comes at the expense of natural and seminatural lands, leading to ecological issues such as habitat destruction, water scarcity, and biodiversity loss (Zhao et al., 2006; An et al., 2023). It also indirectly affects ecosystem functions by encroaching on ecological lands.

*Corresponding author: HUANG Chenlu (E-mail: nwuhcl@163.com)
Received 2024-07-26; revised 2024-11-10; accepted 2024-11-14
© Xinjiang Institute of Ecology and Geography, Chinese Academy of Sciences, Science Press and Springer-Verlag GmbH Germany, part of Springer Nature 2025

China is currently in a phase of rapid urbanization, where regional development imbalances result in better environmental quality in developed regions, whereas underdeveloped regions face high energy consumption and severe pollution, leading to environmental degradation (Ahmad et al., 2020). The green development of urban agglomerations in underdeveloped regions is particularly important because of their potential for significant future economic growth (Hu et al., 2024). Therefore, this study focused on the Guanzhong Plain Urban Agglomeration (GPUA), an essential urban cluster in northwestern inland China, which plays a critical role in ecological protection and high-quality development in the Yellow River Basin, China (Yang et al., 2024). In recent years, the Chinese government has implemented a series of ecological protection and sustainable development policies in the GPUA to address the environmental challenges associated with urbanization. However, as urbanization progresses, urban expansion and land use changes continue to threaten the ecological environment (Fang et al., 2021; Li et al., 2023). Thus, achieving a balance between ecological protection and economic development during urbanization has become a hot research topic.

Net primary productivity (NPP) is the difference between the total organic matter produced by plants through photosynthesis by absorbing carbon dioxide from the atmosphere and the part consumed by autotrophic respiration (Whittaker and Likens, 1975). It reflects the carbon sequestration capability of vegetation and measures the productivity and health of ecosystems. NPP not only plays a crucial role in the carbon cycle but also significantly impacts climate change and ecosystem services (Liu et al., 2019). Understanding the spatiotemporal variation and driving factors of NPP is essential for assessing and managing ecosystem health. The GPUA is an important urban agglomeration and commodity grain production area in northwestern inland China (Yang and Su, 2022), and studying NPP in the region is highly important for regional ecological protection and sustainable development. In recent years, many scholars have studied NPP in China using various methods. For example, through regression analysis, Piao and Fang (2002) analyzed the spatiotemporal variation in NPP on the Qinghai-Xizang Plateau from 1982 to 1999 and reported that NPP exhibited a fluctuating upward trend that was consistent with the distribution trends of hydrothermal conditions. However, trend analysis cannot quantify the impacts of multiple factors on NPP. Therefore, Feng et al. (2007) estimated China's NPP through modeling, using sensitivity tests to determine the impacts of different variables on NPP. The results revealed that leaf area index (LAI) had the greatest impact on NPP estimates, whereas the influence of climate variables varied by region, season, and vegetation type. However, vegetation changes are influenced by not only climate change but also human activities. Ge et al. (2021) used residual trend analysis of multiple regression to separate the contributions of climate change and human activities to China's NPP. Chen et al. (2023) used the geographical detector (Geodetector) to assess the impacts of climate change and human activities on vegetation in the Yellow River Basin. Currently, research methods for NPP are continuously innovating, with significant achievements in regression analysis, modeling, and geospatial detection. However, the application of machine learning in NPP research is relatively rare and still in the exploratory stage.

With the rapid development of computer science, machine learning algorithms are gradually being applied to geographic and ecological research (Scowen et al., 2021; Pichler and Hartig, 2023). EXtreme Gradient Boosting (XGBoost), an emerging machine learning method, has garnered attention for its efficient computational power and ability to handle complex nonlinear relationships (Chen and Guestrin, 2016). By integrating multiple decision trees, XGBoost can provide highly accurate predictions when dealing with large-scale data and complex ecological features. To further interpret and quantify the importance of features, this paper introduced the SHapley Additive exPlanations (SHAP) method. Based on cooperative game theory, SHAP measures each feature's contribution to model predictions, providing a unified and consistent explanation framework (Kim et al., 2023; Hamilton and Papadopoulos, 2024). It allows for detailed explanations of individual samples, making XGBoost model predictions more transparent and interpretable (Wang et al., 2021; Baptista et al., 2022; Li, 2022). Currently,

regression analysis and one-factor sensitivity analysis are widely used methods in NPP research. These methods are straightforward and provide interpretable insights into the linear relationships between variables and NPP. However, they exhibit limitations when addressing nonlinear relationships (De'ath and Fabricius, 2000; Saltelli and Annoni, 2010). In contrast, the XGBoost method combined with SHAP is capable of capturing complex nonlinear patterns (Ouyang et al., 2024). Although Geodetector is capable of handling nonlinear relationships and has advantages in spatial heterogeneity analysis (Wang and Xu, 2017), its ability to explain feature contributions and manage high-dimensional data is less intuitive and flexible than that of the XGBoost-SHAP approach (Li et al., 2024). For example, in the field of NPP research, the XGBoost-SHAP approach has been employed to identify the primary climatic drivers of the Amazon rainforest (Li et al., 2022). This approach has quantified the importance of temperature, solar radiation, and vapor pressure deficits on NPP, helping researchers better understand how these climatic variables influence spatial variation in NPP. Therefore, compared with traditional feature importance methods, XGBoost-SHAP reveals the importance of features across the entire dataset, identifies key driving factors affecting NPP changes, and offers new methods and perspectives for NPP research.

Therefore, this study obtained the MOD17A3HGF NPP product from the Google Earth Engine (GEE) platform and analyzed the NPP trends from 2001 to 2020 using the Theil-Sen trend analysis, Mann-Kendall trend test, coefficient of variation (CV), and Hurst index. Furthermore, the XGBoost-SHAP method was employed to analyze the feature importance of various driving factors on NPP. The specific objectives of this study are: (1) to investigate the spatiotemporal variation characteristics of NPP in the GPUA from 2001 to 2020; and (2) to quantify the impact of each driving factor on NPP changes. This study contributes to the formulation of environmental protection policies for the GPUA, providing a scientific basis for regional ecological civilization construction and high-quality sustainable development.

2 Materials and methods

2.1 Study area

The GPUA is located in northwestern inland China (33°21′–36°57′N, 104°34′–112°34′E; Fig. 1) and covers a total area of approximately 10.71×10^4 km^2 (Dang et al., 2024). This region spans Shaanxi Province, Shanxi Province, and Gansu Province, with Xi'an City at its center. The terrain slopes from southwest to northeast, bordering the Qinling Mountains to the south and the Loess Plateau to the north, with the central area being the Weihe River Plain. The elevation ranges from 210 to 3753 m, featuring diverse landforms such as plains, mountains, and hills. The region experiences a temperate continental monsoon climate characterized by hot and rainy summers and

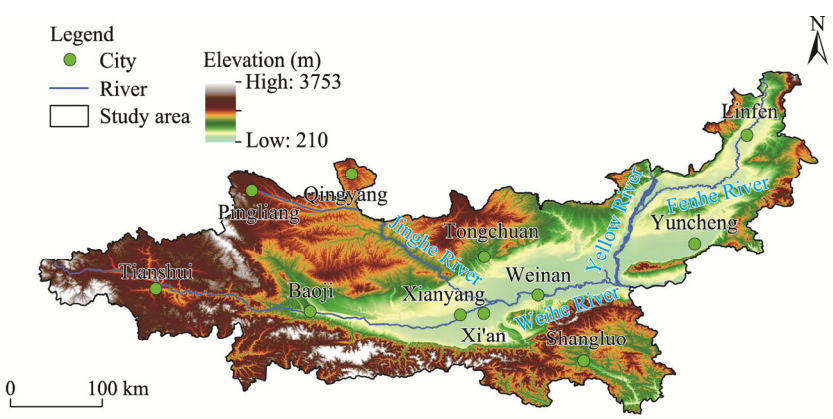

Fig. 1 Overview of the Guanzhong Plain Urban Agglomeration (GPUA) based on the digital elevation model (DEM)

cold, dry winters, with most precipitation occurring during July–September. Major water systems, including the Yellow River, Weihe River, Jinghe River, and Fenhe River, run through the area, along with several nature reserves. The ecological environment in this study area is fragile and significantly impacted by climate change and human activities.

2.2 Data sources

This study employed various datasets to comprehensively analyze the spatiotemporal variation and driving factors of NPP in the GPUA from 2001 to 2020. The primary datasets included MODIS satellite data, climate data, elevation data, land use data, and population density data. The MODIS satellite is suitable for detecting large-scale ecological dynamics and long-term trends, and this study utilized the MOD17A3HGF NPP product data (g C/(m^2·a)) from 2001 to 2020, which were obtained through the GEE platform and batch-exported using the Python API (https://earthengine.google.com/). The climate data included annual average temperature (°C) and annual precipitation (mm) sourced from the National Earth System Science Data Center, National Science & Technology Infrastructure of China (http://www.geodata.cn), specifically from the 1 km resolution annual average temperature dataset and 1 km resolution annual precipitation dataset of China. Elevation data (m) were sourced from the Shuttle Radar Topography Mission (SRTM) digital elevation model (DEM) v3 dataset with a resolution of 30 m, and both slope (°) and aspect (°) data were obtained and processed through the GEE. Land use data were obtained from the China Land Cover Dataset (CLCD) provided by Wuhan University, China (https://doi.org/ 10.5281/zenodo.4417809), with land use types classified into seven categories: cropland, forest, shrubland, grassland, water body, barren land, and impervious surface, all at a resolution of 30 m. Based on previous research on preprocessing methods for land use data (Airiken and Li, 2024), the land use types were reclassified according to vegetation coverage as: barren land, water body, impervious surface, cropland, grassland, shrubland, forest). Annual population density data (persons/hm^2) were derived from the WorldPop dataset that was downloaded via the GEE platform with a spatial resolution of 100 m. WorldPop provides high-resolution population distribution data, facilitating spatial analyses of population density. Additionally, PANDA-China, a long-term series of annual artificial nighttime light datasets for China with a 1 km resolution, helps to better demonstrate the dynamics of long-term human activities. This dataset was obtained through the Big Earth Data Platform for Three Poles (https://poles.tpdc.ac.cn/). Figure 2 shows the spatial distribution of driving factors affecting NPP changes during 2001–2020 in the GPUA.

2.3 Methods

2.3.1 Theil-Sen trend analysis and Mann-Kendall trend test

The Theil-Sen trend analysis method is a nonparametric statistical approach widely used for trend analysis of long time series data. It is particularly effective for analyzing and interpreting trend changes in long-term datasets (Ahmed, 2014). The calculation formula is as follows:

$$\beta = \text{median}\left(\frac{x_j - x_i}{j - i}\right),\ j > i, \tag{1}$$

where β is the Sen's slope of the NPP time series; and x_j and x_i are two data points in the series corresponding to the j^{th} and i^{th} year of the NPP time series (g C/(m^2·a)), respectively. If β>0, it indicates a positive or increasing trend in NPP. Conversely, if β<0, it indicates a negative or decreasing trend in NPP.

The Mann-Kendall trend test is a nonparametric test method that plays a significant role in analyzing long-term time series datasets, particularly in identifying and verifying monotonic trends within the data (Mann, 1945). It determines whether a dataset exhibits a consistent increasing or decreasing trend by comparing the sequential order of data points in the time series. This is especially important for understanding and predicting changes in NPP. The formulas are as follows:

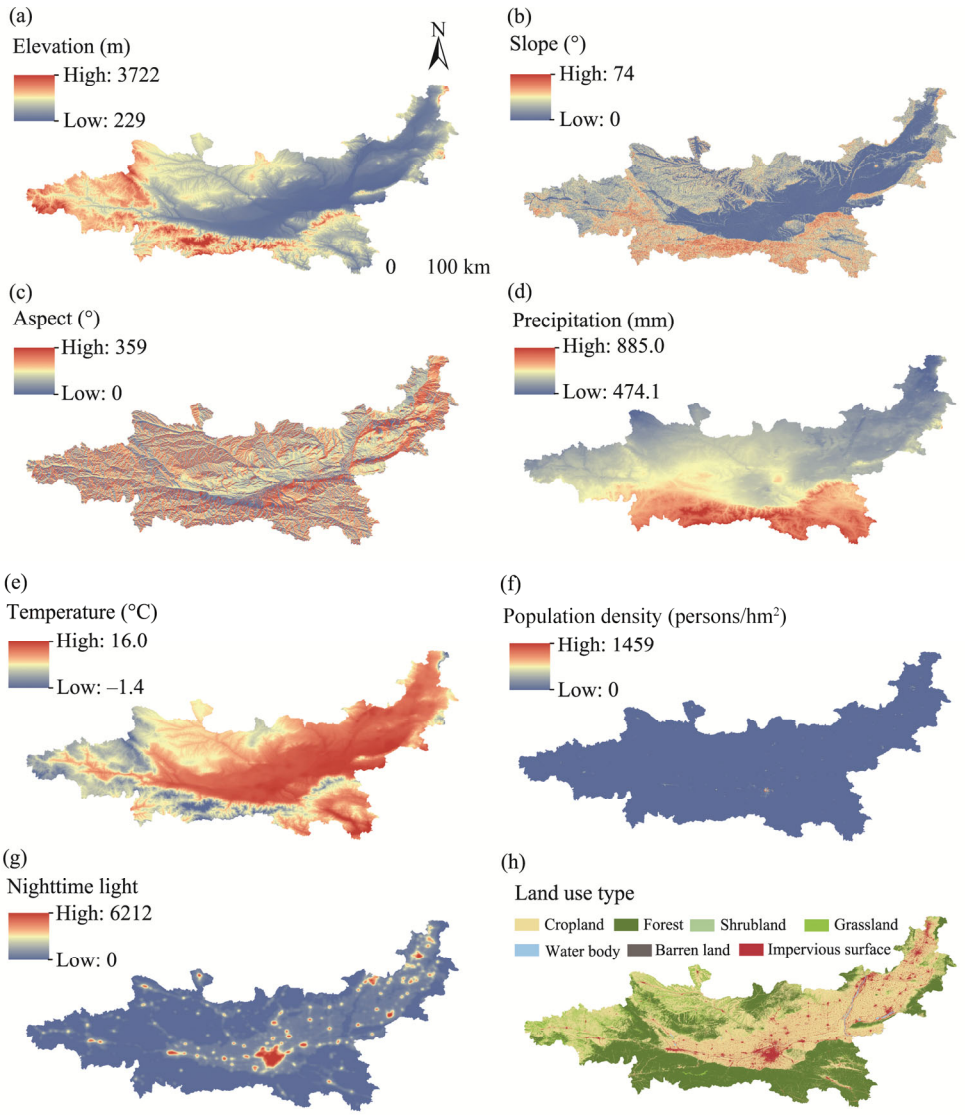

Fig. 2 Spatial distribution of driving factors affecting net primary productivity (NPP) changes during 2001–2020. (a), elevation; (b), slope; (c), aspect; (d), precipitation; (e), temperature; (f), population density; (g), nighttime light; (h), land use type.

$$Z=\begin{cases}\dfrac{S-1}{\sqrt{\mathrm{var}(S)}} & \text{if } S>0\\ 0 & \text{if } S=0\\ \dfrac{S+1}{\sqrt{\mathrm{var}(S)}} & \text{if } S<0\end{cases}, \tag{2}$$

$$S=\sum_{k=1}^{n-1}\sum_{l=k+1}^{n}\mathrm{sgn}\left(x_l-x_k\right), \tag{3}$$

$$\mathrm{sgn}\left(x_l-x_k\right)=\begin{cases}1 & \text{if } x_l-x_k>0\\ 0 & \text{if } x_l-x_k=0\\ -1 & \text{if } x_l-x_k<0\end{cases}, \tag{4}$$

$$\mathrm{var}(S)=\frac{n(n-1)(2n+5)}{18}, \tag{5}$$

where Z is the standardized test statistic; S represents the test statistic; var(S) is the variance of S; n is the length of the NPP time series; and x_l and x_k represent the NPP values for the l^{th} and k^{th} year of the time series (g C/(m^2·a)), respectively. $Z_{1-\alpha/2}$ is the value corresponding to the distribution table of the standard normal distribution function at significance level α. If $|Z|>Z_{1-\alpha/2}$, the hypothesis of no trend is rejected at the significance level of α, and there is an obvious change trend of the time series. When $|Z|>1.96$ and $|Z|>2.58$, the trend is significant at $P<0.05$ and $P<0.01$ levels, respectively.

Based on the trend analysis and significance test results, we divided the change trends of NPP into six categories as described in Table 1.

Table 1 Classification criteria for the change trends of net primary productivity

Sen's slope	*P*	Change trend	Sen's slope	*P*	Change trend
>0	<0.01	Highly significant increase	<0	≥0.05	Non-significant decrease
>0	0.01–0.05	Significant increase	<0	0.01–0.05	Significant decrease
>0	≥0.05	Non-significant increase	<0	<0.01	Highly significant decrease

2.3.2 Calculation of CV

The CV can be used to measure the stability and dispersion of long-term NPP data (Wang et al., 2023). A low CV indicates that NPP in an ecosystem is relatively stable, whereas a higher CV indicates greater fluctuations. The calculation formula is as follows:

$$\mathrm{CV}=\frac{\sigma}{\mu}, \tag{6}$$

where CV is the coefficient of variation; σ represents the standard deviation of the NPP values (g C/(m^2·a)); and μ represents the average NPP value (g C/(m^2·a)). The CV was divided into four levels in the study: very stable (CV≤0.1), stable (0.1<CV≤0.2), unstable (0.2<CV≤0.3), and very unstable (CV>0.3).

2.3.3 Hurst index

The Hurst index is a statistical tool used to measure the long-term memory of time series data. It predicts future trends in a time series dataset through rescaled range analysis (Chamoli et al., 2007). The calculation formula is as follows:

$$H=\frac{\log\left(R/\mathrm{SD}\right)}{\log\left(n\right)}, \tag{7}$$

where H is the Hurst index, typically ranging between 0.0 and 1.0; R is the range (the difference between maximum and minimum cumulative deviations); and SD is the standard deviation (showing data spread). When Hurst index=0.50, the series is a pure random walk (no memory). When Hurst index>0.50, the series has persistence or trend-enhancing characteristics. When Hurst index<0.50, the series has anti-persistence or trend-diminishing characteristics. The closer the Hurst index is to 0.00, the more significant the negative persistence; the closer it is to 1.00, the more significant the positive persistence.

2.3.4 XGBoost gradient boosting algorithm

XGBoost, proposed by Chen and Guestrin in 2016, is an efficient gradient boosting algorithm widely used for regression and classification problems (Chen and Guestrin, 2016). This algorithm is renowned for its high accuracy, parallel computing capabilities, memory optimization, and efficient handling of sparse data. Although XGBoost typically outperforms linear models in terms of predictive performance, it has lower interpretability (Sagi and Rokach, 2021). The workflow of XGBoost includes the following steps: initializing the model, defining the loss function,

calculating gradients and second-order derivatives, constructing new trees, updating predictions, and iterative training (Kavzoglu and Teke, 2022). After training a model using XGBoost, feature importance ranking is an effective method for understanding the model's prediction mechanism. By determining which features contribute most to the model's predictions, feature importance ranking provides valuable insights into the data and model behavior. The dataset was divided into two parts, with 70.00% allocated to the training set and the remaining 30.00% to the testing set (Fig. 3). The XGBoost machine learning model was implemented using Python, with the following key parameters: learning rate (0.1), n_estimators (1000), max_depth (16), and subsample (0.8). Figure 4 shows the prediction results of NPP using the XGBoost model. The predicted values demonstrated a high correlation with the measured values, with a coefficient of determination (R^2) of 0.79, mean absolute error (MAE) of 48.84, and root mean square error (RMSE) of 65.89, indicating good predictive accuracy for NPP in the GPUA.

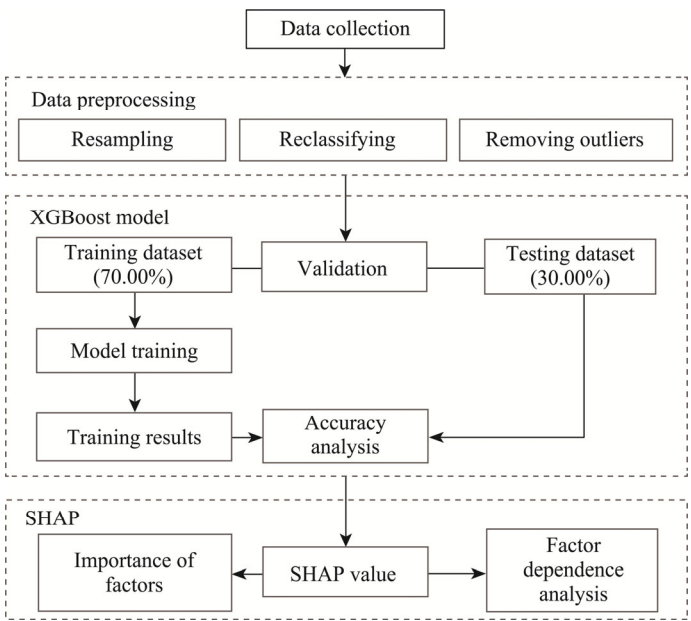

Fig. 3 Flowchart of the XGBoost-SHAP model. XGBoost, eXtreme Gradient Boosting; SHAP, SHapley Additive exPlanations.

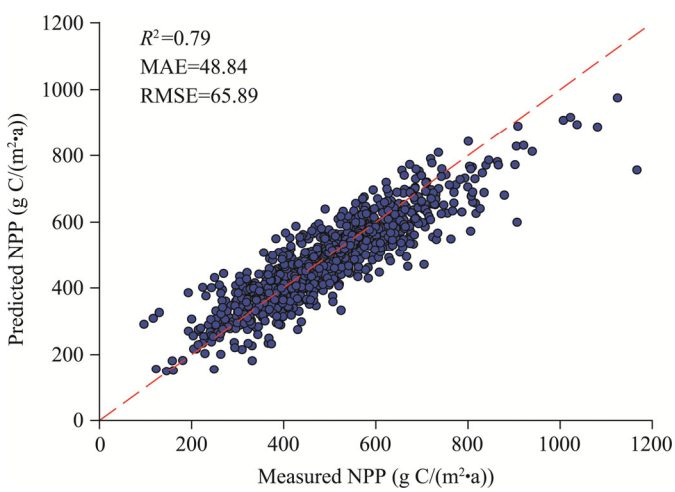

Fig. 4 Accuracy evaluation of predicted NPP in the XGBoost model. MAE, mean absolute error; RMSE, root mean square error.

2.3.5 SHAP method

With improvements in the computational power of machine learning, models are becoming increasingly complex, making it difficult to understand their internal mechanisms and decision-making processes (Ma and Sun, 2020). Consequently, despite performing well during training, models may perform poorly in real-world applications (Hassija et al., 2024). This issue is particularly significant in high-risk applications. Scholars generally agree that high predictive accuracy alone is insufficient to ensure the reliability of models (Tufail et al., 2023). Enhancing the interpretability of "black-box" models and enabling people to understand the reasons behind predictions is crucial for increasing the widespread applicability and trustworthiness of machine learning algorithms.

To address this challenge, Lundberg and Lee (2017) proposed the SHAP, a widely used method inspired by cooperative game theory, to explain the prediction results of various models (both classification and regression models), especially those of "black-box" models that are difficult to interpret. SHAP quantifies the contribution of each feature to the model's predictions and explains the predictions by summing the Shapley values for each input feature. The formula is as follows:

$$g(x') = \phi_0 + \sum_{q=1}^{M} \phi_q x'_q, \tag{8}$$

where $g(x')$ represents the model's prediction value (g C/(m^2·a)); ϕ_0 is the constant that explains the model (the mean prediction value of all training samples) (g C/(m^2·a)); M is the number of simplified input features considered by the SHAP method; ϕ_q is the Shapley value for feature q (the contribution allocated to each feature) (g C/(m^2·a)); and x'_q is the value of the q^{th} simplified input feature in the transformed feature space. This study used the shap.TreeExplainer and shap_values functions in Python 3.0 to identify the influence of driving factors on the model's prediction results. For simplicity and to highlight feature values in the plots, 10,000 data points were randomly selected for SHAP plotting after training.

3 Results

3.1 Spatiotemporal variation in NPP in the GPUA

Figure 5 shows that the average NPP in the GPUA showed an overall increasing trend during 2001–2020, with a cumulative increase of 216.75 g C/(m^2·a) and an average annual increase of 10.84 g C/(m^2·a). The multi-year average NPP value during this period was 484.83 g C/(m^2·a). In 2001, the average NPP was the lowest, at only 340.02 g C/(m^2·a). Starting in 2004, the average NPP showed a fluctuating upward trend, reaching its peak at 573.20 g C/(m^2·a) in 2018. The spatial distribution of multi-year average NPP in the GPUA exhibited a pattern of "higher in the southwest and lower in the northeast" (Fig. 6). The high NPP areas were distributed in the Qinling Mountains in the southwest, whereas the low NPP areas were concentrated in the cropland and built-up areas in the flat central and northeastern regions, as well as the high-altitude mountain planting areas of the western region.

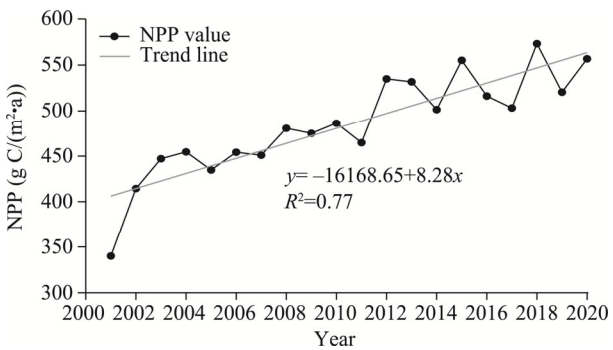

Fig. 5 Temporal variation in average NPP in the GPUA from 2001 to 2020

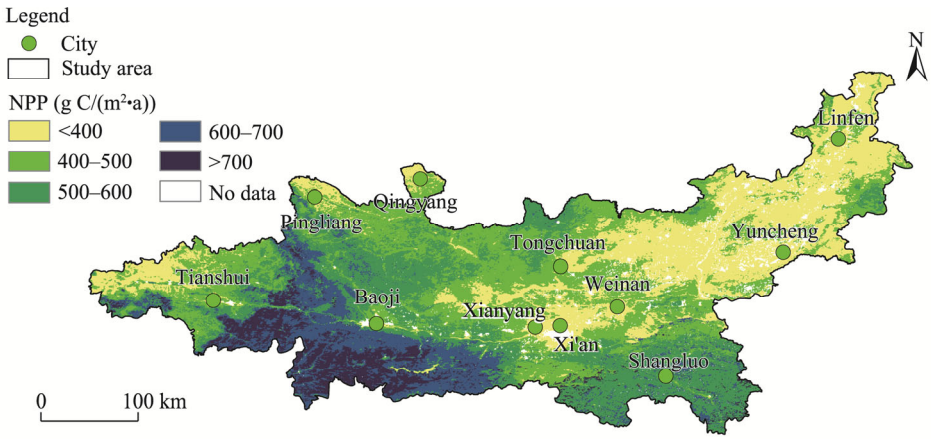

Fig. 6 Spatial variation in multi-year average NPP in the GPUA during 2001–2020

3.2 Trends of NPP in the GPUA

Figure 7 shows the spatial change trends of NPP in the GPUA. From 2001 to 2020, the NPP in the GPUA showed a significant upward trend. Specifically, areas with an increase in NPP accounted for 98.45% of the study area; areas with significant increase in NPP accounted for 32.83% of the study area; areas with highly significant increase in NPP accounted for 22.54% of the total area, and were concentrated in the northwestern part of the study area. Areas with a decrease in NPP accounted for 1.55% of the study area; areas with significant decrease in NPP accounted for 0.19% of the total area; areas with highly significant decrease in NPP accounted for 0.30% of the total area, which were mainly distributed around urbanized regions.

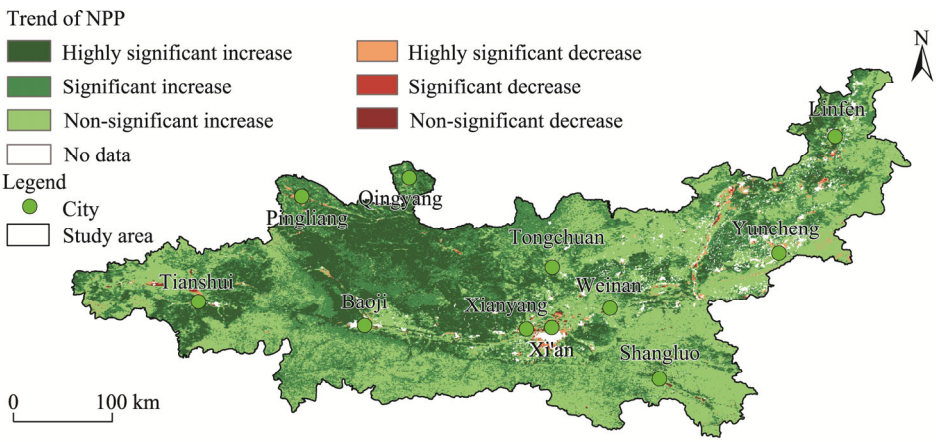

Fig. 7 Spatial variation in the trend of annual NPP in the GPUA during 2001–2020

3.3 Stability of NPP in the GPUA

This study used the CV to analyze the dispersion and fluctuation of NPP over a long time series. As shown in Figure 8, during 2001–2020, the CV of NPP in the GPUA ranged from 0.03 to 0.63, with an average value of 0.14, indicating that the NPP in the study area was relatively stable spatially. Specifically, the very stable areas accounted for 17.84% of the total area, the stable areas accounted for 74.18% of the total area, the unstable areas accounted for 7.40% of the total area, and the very unstable areas accounted for 0.58% of the total area. The unstable areas were distributed mainly along the high-altitude ridgelines and peaks, as well as in the low-altitude areas near the Yellow River Basin and around urban expansion areas.

Fig. 8 Spatial variation in coefficient of variation (CV) in the GPUA during 2001–2020

3.4 Future trend in NPP changes in the GPUA

As shown in Figure 9, the Hurst index of NPP in the study area ranged from 0.12 to 0.95, with an average value of 0.45. Regions with Hurst index below 0.50 accounted for 72.72% of the study area; specifically, regions with Hurst index between 0.00 and 0.30 occupied 2.10% of the total area, and regions with Hurst index between 0.30 and 0.50 accounted for 70.62% of the total area. The NPP time series in the GPUA mainly exhibited weak persistence or weak anti-persistence, suggesting that the growth trend of NPP is difficult to sustain and NPP in most areas is likely to show a decreasing trend in the short term. Regions with Hurst index between 0.50 and 0.70 accounted for 26.93% of the study area, whereas regions with Hurst index above 0.70 accounted for only 0.30% of the study area. The areas exhibiting positive persistent trends were distributed mainly in the western part of the study area and the northern Qinling Mountains, indicating that the vegetation in these areas is likely to improve continuously in the future.

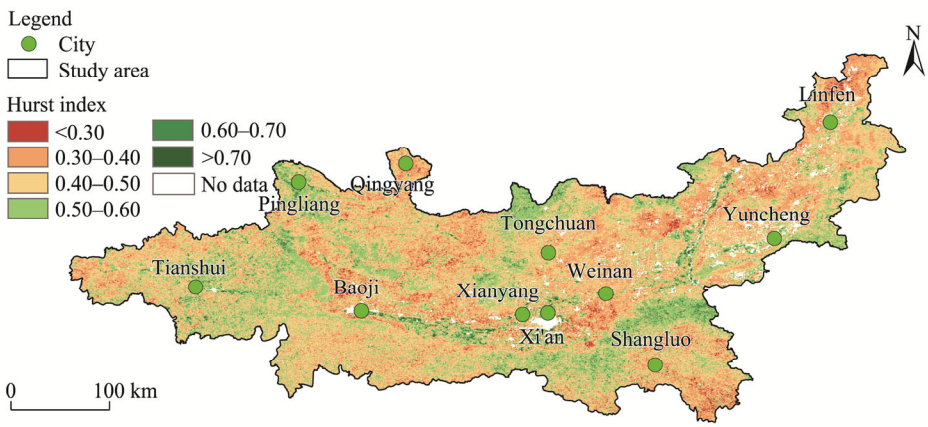

Fig. 9 Spatial variation in Hurst index in the GPUA during 2001–2020

3.5 Importance analysis of factors driving the NPP changes in the GPUA

To further quantify the contribution of each driving factor of NPP, SHAP analysis was performed on NPP and the driving factor datasets to evaluate the importance of each factor. As shown in Figure 10, ranked by contribution, the factors are as follows: elevation, land use type, precipitation, population density, nighttime light, temperature, slope, and aspect. Among these factors, elevation, precipitation, temperature, and slope showed positive impacts on NPP, whereas population density and nighttime light showed negative impacts on NPP. Land use type and aspect were nonlinear data. Among them, the land use type of forest was more conducive to maintaining and promoting vegetation growth, while the contributions of north-facing and east-facing slopes were slightly higher.

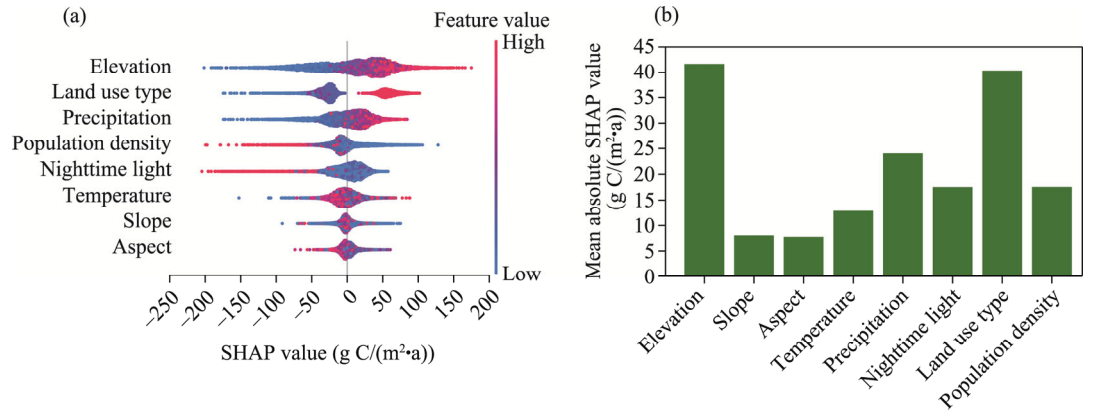

Fig. 10 SHAP value impact plot of the XGBoost model (a) and bar plot showing the mean absolute SHAP values of each driving factor of NPP (b)

3.5.1 Influence of topographical factors on NPP

Elevation, slope, and aspect are all geomorphological factors that influence NPP, but they significantly differ. Visualization of the dependence plots for these three factors using the SHAP algorithm revealed that the impact of elevation on NPP gradually increased with elevation (Fig. 11a). In low-altitude regions (<1000 m), elevation had a negative impact on NPP. However, as elevation increased, elevation had a significantly positive impact on NPP in the mid-to-high altitude range (>1000 m), peaking at 2500 m. Beyond 2500 m, the contribution of elevation to NPP began to weaken and showed a declining trend.

The impact of slope on NPP was relatively small, with a contribution rate close to zero (Fig. 11b). Slope had a considerable effect on low-slope (<10°) regions, where SHAP values were unstable and scattered. As the slope increased, the SHAP values gradually stabilized and slowly increased in the mid-slope range (10°–40°). In high-slope (>40°) regions, the SHAP values again diverged significantly, indicating that the impact of high slopes on NPP is more complex and varied.

The impact of aspect on NPP was minimal and varied across different orientations (Fig. 11c). The north-facing slopes (0°–45° and 315°–360°) had relatively positive SHAP values. The south-facing slopes (135°–225°) tended to exhibit neutral or slightly negative SHAP values, suggesting a less favorable impact on NPP. In addition, the east-facing slopes (45°–135°) and west-facing slopes (225°–315°) displayed more stable SHAP values, with the east-facing slopes generally contributing slightly more than the west-facing slopes.

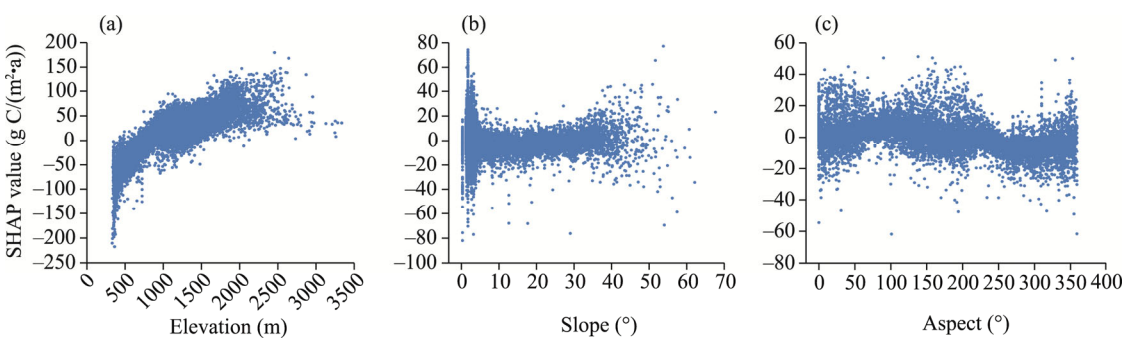

Fig. 11 SHAP dependence plots of elevation (a), slope (b), and aspect (c)

3.5.2 Influence of climate factors on NPP

According to the SHAP dependence plots (Fig. 12a), annual precipitation in the range of 400.0–1100.0 mm had varying impacts on NPP. In the low precipitation range (400.0–500.0 mm), the SHAP values were mostly negative, indicating that precipitation had a negative impact on

NPP in this range. In the moderate precipitation range (500.0–800.0 mm), the SHAP values gradually increase, peaking at approximately 800.0 mm. In this range, the positive impact of precipitation on NPP strengthened as precipitation increased. In the high precipitation range (800.0–1100.0 mm), the SHAP values exhibited a fluctuating trend. The influence of high precipitation on NPP was complex, and its positive impact diminished when precipitation exceeded 950.0 mm.

The impact of temperature on NPP showed a complex nonlinear increasing trend but has a relatively small effect on NPP. Figure 12b illustrates the response of NPP to temperature. In the low-temperature range (0.0°C–7.5°C), the SHAP values were mostly negative. As the temperature increased, the SHAP values tended to increase but remained in the negative range overall, indicating that low temperatures primarily had a negative impact on NPP. In the moderate temperature range (7.5°C–12.5°C), the SHAP values showed a downward trend but overall approached zero, indicating that temperature had a minimal impact on NPP in this range. In the high-temperature range (>12.5°C), the SHAP values increased significantly with increasing temperature, indicating that high temperatures had an increasingly positive impact on NPP.

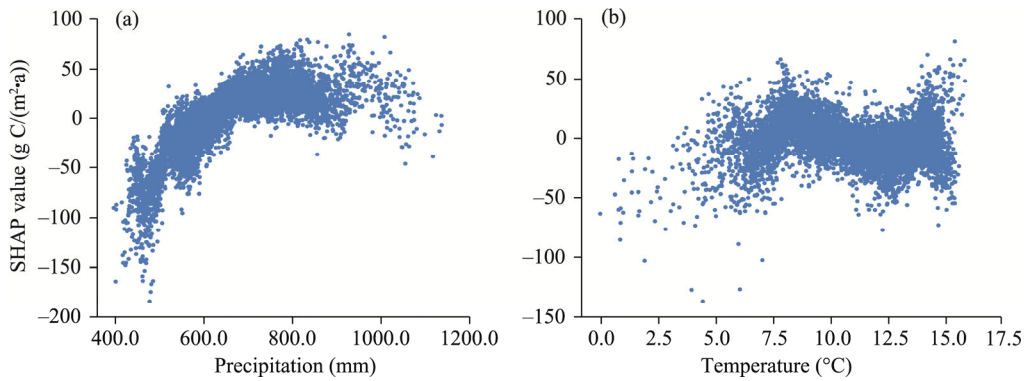

Fig. 12 SHAP dependence plots of precipitation (a) and temperature (b)

3.5.3 Influence of anthropogenic factors on NPP

Both nighttime light and population density had negative impacts on NPP (Fig. 13). In the low nighttime light range (0–10), the SHAP values fluctuated significantly, indicating that the impact of nighttime light on NPP was unstable in this range (Fig. 13a). In the mid-to-high nighttime light range (10–60), the SHAP values showed a continuous downward trend, meaning that the negative impact of nighttime light on NPP intensified as nighttime light values increased. The overall impact of population density on NPP was negative (Fig. 13b). When population density was zero, the SHAP values fluctuated greatly; when population density was greater than zero, the SHAP values were predominantly negative and showed a continuous downward trend as population density increased.

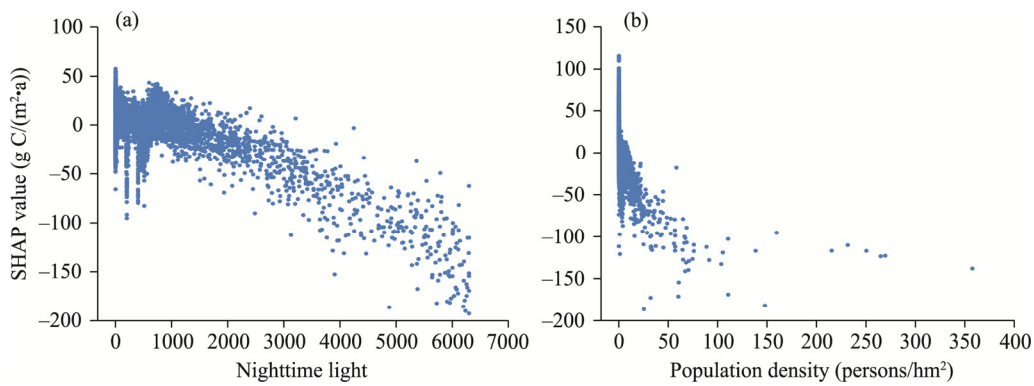

Fig. 13 SHAP dependence plots of nighttime light (a) and population density (b)

4 Discussion

4.1 NPP changes in the GPUA

The GPUA, which covers the provinces of Shaanxi, Gansu, and Shanxi, is the second largest urban cluster in northwestern China. Driven by the "Belt and Road" initiative and the high-quality development strategy of the Yellow River Basin, the region has experienced rapid economic development (Dang et al., 2024). However, this development has created challenges such as weak ecological carrying capacity, water scarcity, soil erosion, and soil pollution (Yang et al., 2022). To address these environmental challenges, Shaanxi and Gansu provinces initiated the Grain for Green Project in 1999, halting cultivation on eroded, low-yield farmland to restore vegetation (Bullock and King, 2011).

This study indicated that since 2000, NPP in the GPUA has shown an increasing trend annually and has maintained a relatively stable spatial state, demonstrating that the Grain for Green Project has significantly improved local vegetation conditions. Additionally, the soil and water conservation projects on the northern Loess Plateau, which lies to the north of the GPUA, have not only reduced soil erosion through large-scale vegetation restoration but also enhanced the stability of the local ecosystem (Zhang et al., 2023), actively contributing to vegetation improvement in the Guanzhong Plain and its surrounding areas. Urban greening policies and natural forest protection policies have also played important roles in improving NPP of the GPUA. Urban greening policies have increased greening coverage and improved the urban ecological environment; meanwhile, natural forest protection policies have promoted the restoration of forest vegetation and soil conservation, reducing human disturbance. The implementation of these policies contributes to the sustainable improvement of vegetation in urbanized areas and natural forest regions in the future (Feng et al., 2021). However, the anti-persistence trend indicated by the Hurst index suggested potential future degradation. This is particularly concerning in northeastern areas with lower average NPP and strong anti-persistence, such as the rapidly developing cities of Weinan and Yuncheng in Shaanxi, where the ecological environment is fragile and the capacity to sustain NPP growth is relatively weak. Future management efforts should focus on areas with strong anti-persistence effects to ensure continued ecological stability.

4.2 Driving factors of NPP in the GPUA

4.2.1 Natural driving factors

This study found that elevation had a significant positive impact on NPP, especially in the southwestern part of the study area, where the elevation of the Qinling Mountains is generally greater than 1000 m. This region, with extensive forest, minimal human disturbance, and better ecological environment, has high vegetation coverage, resulting in high NPP values. Favorable ecological conditions and a suitable climate in high-altitude regions promote plant growth and photosynthesis, significantly increasing NPP. In contrast, low-altitude regions (<1000 m) had negative SHAP values. The central and eastern parts of the GPUA, characterized by low and flat terrain, mainly consist of cropland and built-up areas. Land use changes driven by urban expansion have introduced substantial human disturbances to ecosystems, leading to relatively low NPP values across extensive plain areas. Related research indicated that as the elevation gradient increases, human disturbance decreases, leading to greater vegetation coverage and improved vegetation health (Gao et al., 2019), which is consistent with the findings of this study. On the other hand, the SHAP values for NPP exhibited significant fluctuations when the slope was zero. This is because flat areas (with slope close to zero) primarily include cropland and built-up areas, which are heavily impacted by human activities. Especially during urbanization, varying land use types and vegetation coverage result in high heterogeneity of NPP in these regions. In mid-slope regions (10°–30°), soil moisture and temperature are suitable for vegetation growth, leading to higher vegetation coverage and less soil erosion, resulting in more stable response of NPP to slope. In high-slope regions (>40°), the SHAP values significantly diverged.

Although some high SHAP values might be due to good ecological conditions in high-altitude regions, offsetting the negative impacts of steep slopes, the overall negative impact of high slopes remains significant. The adverse effects of high slopes include increased soil erosion, reduced soil moisture, and nutrient loss, which collectively restrict plant growth and decrease NPP (Berhe et al., 2007), causing large fluctuations in SHAP values in high-slope regions. Moreover, the impact of aspect on NPP was also variable and inconsistent. North-facing slopes receive less direct sunlight, resulting in cooler temperatures and higher soil moisture, which creates favorable conditions for vegetation growth, especially in high-altitude regions, increasing NPP. In contrast, south-facing slopes receive more solar radiation, leading to higher temperatures, drier soils, and faster water loss, which limits vegetation growth. East-facing slopes benefit from early morning sunlight and higher humidity, promoting photosynthesis and creating better growth conditions. West-facing slopes are generally drier, causing greater water stress on plants, making their growth conditions less favorable than those on east-facing slopes (Singh, 2018).

Precipitation and temperature are major factors influencing NPP under climate change (Yuan et al., 2021). This study indicated that annual precipitation within the range of 400.0–1100.0 mm significantly affected NPP. In the low-precipitation range (400.0–500.0 mm), precipitation mainly negatively impacted NPP. For annual precipitation less than 500.0 mm, vegetation growth is significantly constrained, and the LAI shows a marked decline, indicating a reduction in vegetation coverage. Furthermore, insufficient precipitation results in inadequate soil moisture replenishment, further inhibiting normal plant growth processes and disrupting the water balance of the ecosystem (Wu et al., 2020; Chen and Zhang, 2023). In the moderate precipitation range (500.0–800.0 mm), the SHAP values gradually increase, peaking at approximately 800 mm. In this range, the positive impact of precipitation on NPP strengthened with increasing precipitation. In the high precipitation range (800.0–1100.0 mm), the SHAP values exhibited a fluctuating trend. The complex impact of high precipitation on NPP diminished its positive effect when precipitation exceeded 950 mm. This could be due to overly wet soil conditions causing poor drainage, root hypoxia, and nutrient leaching, ultimately inhibiting the increase in NPP (Kaur et al., 2020). This study demonstrated that suitable precipitation is crucial for increasing NPP in the GPUA, whereas both extreme and insufficient water conditions inhibit NPP growth. The complex nonlinear impact of temperature on NPP reflected differences in plant growth under varying temperature conditions. Under low temperatures, plant photosynthesis and growth are inhibited, significantly limiting NPP values. Moderate temperatures (5.0°C–12.5°C) increase photosynthetic efficiency, significantly increasing NPP. However, under relatively high-temperature conditions, although their photosynthetic efficiency continues to improve, plants may approach their optimal growth temperature (Hatfield and Prueger, 2015). In the central and northeastern plain areas, high temperatures are often accompanied by insufficient precipitation, leading to drought, which inhibits vegetation growth. In contrast, in the eastern Qinling Mountains, high temperatures bring more precipitation, promoting vegetation photosynthesis and growth, but the impact on NPP also diminishes once precipitation reaches a threshold. Although further increases in temperature will still have a positive effect on NPP, the rate of increase will decrease.

4.2.2 Anthropogenic driving factors

Driven by the "Belt and Road" initiative and the high-quality development strategy of the Yellow River Basin, the social and economic development of the GPUA has rapidly advanced. However, land use changes, primarily due to urban expansion, have exerted tremendous pressure on the region's ecological environment. These changes have not only destroyed natural vegetation but also exacerbated problems such as soil erosion and pollution, impacting the stability and sustainable development of regional ecosystems (Ye et al., 2023). This impact is reflected in the negative effects of nighttime light and population density on NPP, as nighttime light and population density are anthropogenic factors that affect the ecological environment (Zhao et al., 2022; Kang et al., 2023). Areas with strong nighttime light are typically cities and their surrounding areas. These areas experience frequent human activities, which negatively impact

vegetation coverage and ecosystems, leading to lower NPP values. High population density indicates increased land use intensity and frequency of human activities, which are often accompanied by significant land use changes, such as the conversion of cropland to construction land. This shift increases resource consumption and environmental pollution, inhibiting vegetation growth.

The land use type in the GPUA was predominantly cropland, which accounted for more than 40.00% of the area. Impervious surface, surrounded by cropland, accounted for less than 7.00% of the area (Table 2). Grassland and forest were distributed in relatively high-altitude regions in the northwest and south, covering 46.53% of the study area. The proportion of impervious surface significantly increased from 2001 to 2020, rising from 3.49% to 6.22% of the study area, an expansion of 2894.91 km^2, with an urban area growth of 48.82%, and the growth rate accelerated after 2010. Moreover, the area of cropland showed a decreasing trend, dropping from 53,614.92 km^2 in 2001 to 50,035.97 km^2 in 2020, a total reduction of 3578.95 km^2. This shift in land use types is due mainly to the encroachment of cropland by impervious surface during urban expansion. The accelerated urbanization process has severely affected the quality of the regional ecological environment. As a result, the NPP values in low-altitude central and eastern regions were low because of the impacts of urban expansion and high-intensity human activities. However, human activities can also have positive effects on ecological environment. Through the implementation of ecological restoration policies, such as returning cropland to forest and grassland, vegetation in some areas of the GPUA has been restored and improved. Since 2000, policies for returning cropland to forest and afforestation have increased forest area from 34,456.85 km^2 in 2001 to 38,838.13 km^2 in 2020, an increase of 4381.28 km^2. These measures not only increase vegetation coverage and carbon sequestration capacity but also improve soil structure, reduce soil erosion, and promote ecosystem restoration. Therefore, despite the significant negative impacts of human activities on areas surrounding cities, reasonable ecological protection and restoration measures have greatly improved the ecological environment in most regions, promoting the healthy development of regional ecosystems.

Table 2 Land use transition matrix (unit: km^2) in the GPUA during 2001–2020

	Cropland	Forest	Shrubland	Grassland	Water body	Barren land	Impervious surface
Cropland	45,615.23	1749.60	5.11	3278.88	149.06	3.21	2813.82
Forest	580.16	33,808.78	14.88	45.42	0.18	0.02	7.40
Shrubland	17.86	372.74	54.71	61.81	0.00	0.00	0.03
Grassland	3714.82	2906.45	48.90	7625.97	10.22	0.91	80.92
Water body	78.21	0.53	0.00	0.77	204.97	0.20	48.78
Barren land	0.59	0.00	0.00	0.54	2.85	0.90	2.04
Impervious surface	29.09	0.03	0.00	0.46	89.97	0.23	3709.85

4.3 Shortcomings and prospects

This study systematically analyzed the spatiotemporal variation in NPP and the feature contributions of its driving factors in the GPUA. However, there are certain limitations. Although the analysis revealed the impacts of changes caused by natural factors and human activities on NPP, the accuracy of the results is somewhat constrained by the use of a single model. Future research could incorporate other machine learning models, such as Categorical Boosting (CatBoost) and Light Gradient Boosting Machine (LightGBM), to conduct cross-validation across multiple models and enhance the reliability of the results. In addition, the MOD17A3HGF NPP product has relatively low spatial resolution, making it difficult to capture localized heterogeneity and small-scale ecological changes in the analysis of NPP changes. Furthermore, the selection of driving factors in this study is limited by data availability, and future research should consider a

broader range of driving factors. Another limitation is the lack of in-depth analysis of the spatial heterogeneity of the driving factors in this study. Although we assessed the overall impact of the driving factors, we did not explore their variations and differences across different regions or cities. Additionally, this study employed only a single-factor analysis of driving factors of NPP, without considering the interactions among features. This may lead to an incomplete understanding of the driving factors of NPP, as many ecological processes are complex and influenced by interactions among factors. Future research should address these two aspects by focusing on detailed analyses of different regions and exploring interaction factor analysis to achieve a more comprehensive understanding of the spatial differences and combined effects of driving factors.

Despite these limitations, the XGBoost-SHAP method provides new tools and perspectives for future ecological research. Its high precision and strong predictive power offer more accurate and reliable prediction results. Moreover, its ability to handle large-scale, multisource data is highly significant for ecological research on large-scale regions with multidimensional data. Overall, this study contributes to a better understanding of the drivers and mechanisms behind NPP changes in the GPUA.

5 Conclusions

This study revealed the response of NPP to climate change and human activities in the GPUA based on an in-depth analysis of spatiotemporal varition in NPP during 2001–2020. The following conclusions are drawn from Theil-Sen trend analysis, Mann-Kendall trend test, CV, Hurst index, and the XGBoost-SHAP machine learning methods:

(1) During 2001–2020, the average NPP in the GPUA was 484.83 g C/(m^2·a), increasing from 340.02 g C/(m^2·a) in 2001 to 573.20 g C/(m^2·a) in 2020, indicating an overall increasing trend. The spatial distribution of NPP exhibited a pattern of "higher in the southwest and lower in the northeast", with higher values in the Qinling Mountains in the southwest. The low-value areas were concentrated in the cropland and built-up areas in the flat central and northeastern regions, as well as the high-altitude mountain planting areas in the west.

(2) The average CV of NPP in the GPUA was 0.14, indicating that NPP was generally relatively stable. However, there were significant fluctuations in the high-altitude ridgelines and peaks, as well as in low-altitude regions near the Yellow River Basin in the northeast and around urban expansion areas. The Hurst index ranged from 0.12 to 0.95, with an average of 0.45. A total of 72.72% of the study area exhibited weak anti-persistence, suggesting that the NPP in most areas may decline in the short term. Future efforts should focus on these areas, strengthening ecological protection and restoration measures to improve the stability of NPP.

(3) Through XGBoost-SHAP analysis, elevation, land use type and precipitation were determined to be the main driving factors of NPP. Elevation and land use changes during the implementation of Grain for Green Project promoted NPP growth, whereas extreme climate conditions and high population density suppressed NPP growth. The response of NPP to climate factors exhibited nonlinear characteristics, with suitable precipitation and higher temperatures contributing to vegetation improvement.

Future research should focus on incorporating more climate variables and their interactions to comprehensively evaluate the response of NPP under complex environmental conditions. In addition, with the continuous advancement of urbanization, future research should pay attention to the refined impacts of human activities on NPP under different urban scales to propose more targeted ecological protection strategies.

Conflict of interest

The authors declare that they have no known competing financial interests or personal relationships that could have appeared to influence the work reported in this paper.

Acknowledgements

This research was funded by the Xi'an Social Science Fund (24QL38).

Author contributions

Conceptualization: LIU Yuke, HUANG Chenlu; Data curation: LIU Yuke, YANG Chun, CHEN Chen; Formal analysis: CHEN Chen, LIU Yuke; Funding acquisition: HUANG Chenlu; Investigation: LIU Yuke, YANG Chun; Methodology: HUANG Chenlu, LIU Yuke; Project administration: YANG Chun; Resources: LIU Yuke, YANG Chun, CHEN Chen; Software: CHEN Chen, HUANG Chenlu; Supervision: HUANG Chenlu; Validation: YANG Chun, CHEN Chen; Visualization: LIU Yuke, YANG Chun, CHEN Chen; Writing - original draft: LIU Yuke. All authors approved the manuscript.

References

Ahmad F, Draz M U, Ozturk I, et al. 2020. Looking for asymmetries and nonlinearities: The nexus between renewable energy and environmental degradation in the northwestern provinces of China. Journal of Cleaner Production, 266: 121714, doi: 10.1016/j.jclepro.2020.121714.

Ahmed S M. 2014. Assessment of irrigation system sustainability using the Theil-Sen estimator of slope of time series. Sustainability Science, 9(3): 293–302.

Airiken M, Li S C. 2024. The dynamic monitoring and driving forces analysis of ecological environment quality in the Tibetan Plateau based on the Google Earth Engine. Remote Sensing, 16(4): 682, doi: 10.3390/rs16040682.

An H, Xiao W D, Huang J. 2023. Relationship of construction land expansion and ecological environment changes in the Three Gorges reservoir area of China. Ecological Indicators, 157: 111209, doi: 10.1016/j.ecolind.2023.111209.

Baptista M L, Goebel K, Henriques E M P. 2022. Relation between prognostics predictor evaluation metrics and local interpretability SHAP values. Artificial Intelligence, 306: 103667, doi: 10.1016/j.artint.2022.103667.

Berhe A A, Harte J, Harden J W, et al. 2007. The significance of the erosion-induced terrestrial carbon sink. BioScience, 57(4): 337–346.

Bullock A, King B. 2011. Evaluating China's Slope Land Conversion Program as sustainable management in Tianquan and Wuqi Counties. Journal of Environmental Management, 92(8): 1916–1922.

Chamoli A, Ram Bansal A, Dimri V P. 2007. Wavelet and rescaled range approach for the Hurst coefficient for short and long time series. Computers & Geosciences, 33(1): 83–93.

Chen T Q, Guestrin C. 2016. XGBoost: A scalable tree boosting system. Proceedings of the 22nd ACM SIGKDD International Conference on Knowledge Discovery and Data Mining. New York: Association for Computing Machinery, 785–794.

Chen X, Zhang Y P. 2023. Impacts of climate, phenology, elevation and their interactions on the net primary productivity of vegetation in Yunnan, China under global warming. Ecological Indicators, 154(7725): 110533, doi: 10.1016/j.ecolind.2023.110533.

Chen Y, Guo D B, Cao W J, et al. 2023. Changes in net primary productivity and factor detection in China's Yellow River Basin from 2000 to 2019. Remote Sensing, 15(11): 2798, doi: 10.3390/rs15112798.

Dang X, Ma B B, Xue D Q, et al. 2024. The spatial pattern of polluting enterprises and the effects of local regulation in the Guanzhong Plain Urban Agglomeration. Land, 13(6): 733, doi: 10.3390/land13060733.

De'ath G, Fabricius K E. 2000. Classification and regression trees: A powerful yet simple technique for ecological data analysis. Ecology, 81(11): 3178–3192.

Fang C L, Liu H M, Wang S J. 2021. The coupling curve between urbanization and the eco-environment: China's urban agglomeration as a case study. Ecological Indicators, 130(4): 108107, doi: 10.1016/j.ecolind.2021.108107.

Feng D R, Bao W K, Yang Y Y, et al. 2021. How do government policies promote greening? Evidence from China. Land Use Policy, 104: 105389, doi: 10.1016/j.landusepol.2021.105389.

Feng X, Liu G, Chen J M, et al. 2007. Net primary productivity of China's terrestrial ecosystems from a process model driven by remote sensing. Journal of Environmental Management, 85(3): 563–573.

Gao M D, Piao S L, Chen A P, et al. 2019. Divergent changes in the elevational gradient of vegetation activities over the last 30 years. Nature Communications, 10(1): 2970, doi: 10.1038/s41467-019-11035-w.

Ge W Y, Deng L Q, Wang F, et al. 2021. Quantifying the contributions of human activities and climate change to vegetation net primary productivity dynamics in China from 2001 to 2016. Science of the Total Environment, 773: 145648, doi: 10.1016/j.scitotenv.2021.145648.

Hamilton R I, Papadopoulos P N. 2024. Using SHAP values and machine learning to understand trends in the transient stability limit. IEEE Transactions on Power Systems, 39(1): 1384–1397.

Hassija V, Chamola V, Mahapatra A, et al. 2024. Interpreting black-box models: A review on explainable artificial intelligence. Cognitive Computation, 16(1): 45–74.

Hatfield J L, Prueger J H. 2015. Temperature extremes: Effect on plant growth and development. Weather and Climate Extremes, 10: 4–10.

Hu W B, Li Z F, Chen D L, et al. 2024. Unlocking the potential of collaborative innovation to narrow the inter-city urban land green use efficiency gap: Empirical study on 19 urban agglomerations in China. Environmental Impact Assessment Review, 104: 107341, doi: 10.1016/j.eiar.2023.107341.

Kang J M, Li C L, Zhang B L, et al. 2023. How do natural and human factors influence ecosystem services changing? A case study in two most developed regions of China. Ecological Indicators, 146(3): 109891, doi: 10.1016/j.ecolind.2023.109891.

Kaur G, Singh G, Motavalli P P, et al. 2020. Impacts and management strategies for crop production in waterlogged or flooded soils: A review. Agronomy Journal, 112(3): 1475–1501.

Kavzoglu T, Teke A. 2022. Advanced hyperparameter optimization for improved spatial prediction of shallow landslides using extreme gradient boosting (XGBoost). Bulletin of Engineering Geology and the Environment, 81(5): 201, doi: 10.1007/s10064-022-02708-w.

Kim J Y, Shin U H, Kim K. 2023. Predicting biomass composition and operating conditions in fluidized bed biomass gasifiers: An automated machine learning approach combined with cooperative game theory. Energy, 280: 128138, doi: 10.1016/j.energy.2023.128138.

Li L N, Xia R, Dou M, et al. 2024. Integrated machine learning reveals aquatic biological integrity patterns in semi-arid watersheds. Journal of Environmental Management, 359(5): 121054, doi: 10.1016/j.jenvman.2024.121054.

Li L Y, Zeng Z Z, Zhang G, et al. 2022. Exploring the individualized effect of climatic drivers on MODIS net primary productivity through an explainable machine learning framework. Remote Sensing, 14(17): 4401, doi: 10.3390/rs14174401.

Li Y K, Li X Z, Lu T. 2023. Coupled coordination analysis between urbanization and eco-environment in ecologically fragile areas: A case study of Northwestern Sichuan, Southwest China. Remote Sensing, 15(6): 1661, doi: 10.3390/rs15061661.

Li Z Q. 2022. Extracting spatial effects from machine learning model using local interpretation method: An example of SHAP and XGBoost. Computers, Environment and Urban Systems, 96(7): 101845, doi: 10.1016/j.compenvurbsys.2022.101845.

Lin X Q, Wang Y, Wang S J, et al. 2015. Spatial differences and driving forces of land urbanization in China. Journal of Geographical Sciences, 25(5): 545–558.

Liu Y Y, Yang Y, Wang Q, et al. 2019. Evaluating the responses of net primary productivity and carbon use efficiency of global grassland to climate variability along an aridity gradient. Science of the Total Environment, 652: 671–682.

Lundberg S M, Lee S I. 2017. A unified approach to interpreting model predictions. In: Advances in Neural Information Processing Systems 30. New York: Curran Associates Inc., 4768–4777.

Ma L Y, Sun B H. 2020. Machine learning and AI in marketing—Connecting computing power to human insights. International Journal of Research in Marketing, 37(3): 481–504.

Mann H B. 1945. Nonparametric tests against trend. Econometrica, 13(3): 245–259.

Ouyang Y, Li X W, Zhou W J, et al. 2024. Integration of machine learning XGBoost and SHAP models for NBA game outcome prediction and quantitative analysis methodology. PLoS ONE, 19(7): e0307478, doi: 10.1371/journal.pone.0307478.

Piao S L, Fang J Y. 2002. Terrestrial net primary production and its spatio-temporal patterns in Qinghai-Xizang Plateau, China during 1982–1999. Journal of Natural Resources, 17(3): 373–380. (in Chinese)

Pichler M, Hartig F. 2023. Machine learning and deep learning—A review for ecologists. Methods in Ecology and Evolution, 14(4): 994–1016.

Sagi O, Rokach L. 2021. Approximating XGBoost with an interpretable decision tree. Information Sciences, 572: 522–542.

Saltelli A, Annoni P. 2010. How to avoid a perfunctory sensitivity analysis. Environmental Modelling & Software, 25(12): 1508–1517.

Scowen M, Athanasiadis I N, Bullock J M, et al. 2021. The current and future uses of machine learning in ecosystem service research. Science of the Total Environment, 799: 149263, doi: 10.1016/j.scitotenv.2021.149263.

Singh S. 2018. Understanding the role of slope aspect in shaping the vegetation attributes and soil properties in Montane ecosystems. Tropical Ecology, 59(3): 417–430.

Tufail S, Riggs H, Tariq M, et al. 2023. Advancements and challenges in machine learning: a comprehensive review of models, libraries, applications, and algorithms. Electronics, 12(8): 1789, doi: 10.3390/electronics12081789.

Wang G J, Peng W F, Zhang L D, et al. 2023. Quantifying the impacts of natural and human factors on changes in NPP using an optimal parameters-based geographical detector. Ecological Indicators, 155(3): 111018, doi: 10.1016/j.ecolind.2023.111018.

Wang J F, Xu C D. 2017. Geodetector: Principle and prospective. Acta Geographica Sinica, 72(1): 116–134. (in Chinese)

Wang K, Tian J, Zheng C, et al. 2021. Interpretable prediction of 3-year all-cause mortality in patients with heart failure caused by coronary heart disease based on machine learning and SHAP. Computers in Biology and Medicine, 137(5): 104813, doi: 10.1016/j.compbiomed.2021.104813.

Whittaker R H, Likens G E. 1975. The Biosphere and Man. In: Lieth H, Whittaker R H. Primary Productivity of the Biosphere. Berlin, Heidelberg: Springer Berlin, Heidelberg, 305–328.

Wu D D, Xie X H, Tong J X, et al. 2020. Sensitivity of vegetation growth to precipitation in a typical afforestation area in the Loess Plateau: Plant-water coupled modelling. Ecological Modelling, 430(16): 109128, doi: 10.1016/j.ecolmodel.2020.109128.

Yang J X, Ma X, Zhao X Y, et al. 2022. Spatiotemporal of the coupling relationship between ecosystem services and human well-being in Guanzhong Plain Urban Agglomeration. International Journal of Environmental Research and Public Health, 19(19): 12535, doi: 10.3390/ijerph191912535.

Yang L, Meng H H, Wang J T, et al. 2024. The vulnerability assessment and obstacle factor analysis of urban agglomeration along the Yellow River in China from the perspective of production-living-ecological space. PLoS ONE, 19(4): e0299729, doi: 10.1371/journal.pone.0299729.

Yang S, Su H. 2022. Multi-scenario simulation of ecosystem service values in the Guanzhong Plain Urban Agglomeration, China. Sustainability, 14(14): 8812, doi: 10.3390/su14148812.

Ye D, Yang L, Zhou M. 2023. Spatiotemporal variation in ecosystem health and its driving factors in Guizhou Province. Land, 12(7): 1439, doi: 10.3390/land12071439.

Yuan Z, Wang Y Q, Xu J J, et al. 2021. Effects of climatic factors on the net primary productivity in the source region of Yangtze. Scientific Reports, 11: 1376, doi: 10.1038/s41598-020-80494-9.

Zhang B Q, Tian L, He C S, et al. 2023. Response of erosive precipitation to vegetation restoration and its effect on soil and water conservation over China's Loess Plateau. Water Resources Research, 59(1): e2022WR033382, doi: 10.1029/2022WR033382.

Zhao S Q, Da L J, Tang Z Y, et al. 2006. Ecological consequences of rapid urban expansion: Shanghai, China. Frontiers in Ecology and the Environment, 4(7): 341–346.

Zhao Y H, Qu Z, Zhang Y, et al. 2022. Effects of human activity intensity on habitat quality based on nighttime light remote sensing: A case study of Northern Shaanxi, China. Science of the Total Environment, 851(126): 158037, doi: 10.1016/j.scitotenv.2022.158037.